



## Regular Article

## Electrospun frogspawn structured membrane for gravity-driven oil-water separation



Mengjie Zhang<sup>a,1</sup>, Wenjing Ma<sup>a,1</sup>, Shutian Wu<sup>a</sup>, Guosheng Tang<sup>a</sup>, Jiaxin Cui<sup>a</sup>, Qilu Zhang<sup>b</sup>, Fei Chen<sup>c</sup>, Ranhua Xiong<sup>d,\*</sup>, Chaobo Huang<sup>a,e,\*</sup>

<sup>a</sup> College of Chemical Engineering, Jiangsu Provincial Key Lab for the Chemistry and Utilization of Agro-forest Biomass Jiangsu Key Lab of Biomass-based Green Fuels and Chemicals, Nanjing Forestry University (NFU), Nanjing 210037, PR China

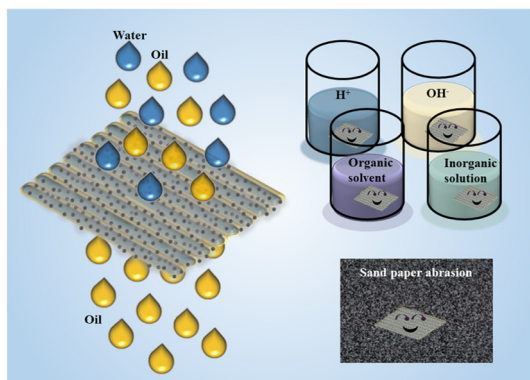
<sup>b</sup> School of Material Science and Engineering, Xi'an Jiaotong University, Xi'an 710049, PR China

<sup>c</sup> Center for Quantitative Synthetic Biology, Institute of Synthetic Biology, Shenzhen Institute of Advanced Technology, Chinese Academy of Sciences, Shenzhen 518055, PR China

<sup>d</sup> Lab General Biochemistry & Physical Pharmacy, Department of Pharmaceutics, Ghent University, 9000, Belgium

<sup>e</sup> Laboratory of Biopolymer Based Functional Materials, Jiangsu Co-Innovation Center of Efficient Processing and Utilization of Forest Resources, Nanjing Forestry University, Nanjing 210037, PR China

## GRAPHICAL ABSTRACT



## ARTICLE INFO

## Article history:

Received 16 November 2018

Revised 28 March 2019

Accepted 29 March 2019

Available online 30 March 2019

## Keywords:

Superhydrophobic

Dip-coating

Electrospun membrane

High stability

Oil-water separation

## ABSTRACT

The aim of this study is to prepare a fibrous membrane scaffold that possesses a frogspawn structure for high-efficiency oil-water separation. Polyamic acid was first electrospun onto a rotating wheel-collector to obtain the fibrous membrane. Subsequently, post-processing by immersion in a polydimethylsiloxane solution and a silica nanoparticles suspension, followed by a thermal treatment generated a frogspawn-structured fibrous membrane. The obtained membrane achieved superhydrophobicity and superoleophilicity, with the water contact angle as high as 155.75° and the oil contact angle lower than 10°. The separation efficiencies of the membrane were higher than 99.55% and the permeate flux was maintained at greater than 4400 L/m<sup>2</sup>·h after 20 separation cycles. Additionally, the wettability studies suggested the membrane exhibits high stability because it can resist damages due to high temperature (150 °C), acid/basic conditions and organic/inorganic solvents. These findings indicated that this composite membrane has great potential for use in gravity-driven oil-water separation and can extend the range of its application for treatments of oil spills incident, oily wastewater and spent liquor.

© 2019 Published by Elsevier Inc.

\* Corresponding authors.

E-mail addresses: [ranhua.xiong@gmail.com](mailto:ranhua.xiong@gmail.com) (R. Xiong), [huangchaobo@njfu.edu.cn](mailto:huangchaobo@njfu.edu.cn) (C. Huang).

<sup>1</sup> These authors contributed equally to this work.

## 1. Introduction

Currently, water pollution problems have given rise to strong repercussions in society, particularly for the oily wastewater pollution [1,2]. The oil leakage at the Gulf of Mexico [3] and ‘Sanchi’ tanker incident [4,5] brought oil pollution into the public eye [6]. Additionally, the oily wastewater from the daily life and the spent liquor containing pollutants such as heavy metal ions [7], and organic dyes [8] from chemical laboratory are both issues that still need to be addressed. Oily pollution not only inconveniences the residents but the scientific community and the government are also alarmed by oily pollution. To solve these problems, physical adsorption [9,10] or separation [11,12], chemical reaction [13], biodegradation [13,14], centrifugal sedimentation [15], and other technologies and methods have been applied [16]. However, these methods either require high energy input or shows limited separation performance [17]. Therefore, development of better separation materials for oil-water separation is urgently needed [18]. Among the variety of materials such as membranes [19,20], foams [21,22], sponges [23,24], and microspheres [25], membranes have been the mostly studied materials because the membranes are easy to prepare and show excellent separation performance [26–29].

Recent efforts have focused on the functionalization of the membrane and the simplification of the membrane preparation process [30,31]. Among the various methods for membrane preparation such as chemical vapour deposition [32], templating [33], gas-spraying [34], and electrospinning [17], electrospinning is one of the most facile and effective methods that has been shown to be easy to control, cost-effective, does not require sophisticated equipment, and provides the membrane with a large surface area [35]. To date, polyvinyl acetate [36], polyacrylonitrile/polyethylene glycol [37], poly (lactic acid) [38] and other polymers [39–41] have been successfully electrospun to fabricate the separation membranes. Meanwhile, the dip-coating method has been utilized in many previous studies [42,43] to modify the membrane [44–48]

for the desired properties. The stabilization of the membrane after the dip-coating can be achieved by using a thermal treatment [20], irradiation [49], chemical reaction/cross-linking [50] and solvent evaporation [51]. All these methods enabled the efficient preparation of membranes.

Hence, inspired by morphology from nature, a frogspawn-structure membrane was fabricated by combining the electrospinning technique with the dip-coating method. Polyimide (PI) which is a high-performance material [52] was used in this study to form the membrane substrate. Subsequently, low surface energy polydimethylsiloxane (PDMS) was introduced onto the PI membrane to form the hydrophobic surface. Furthermore, the silica nanoparticles (SNPs) helped to form the frogspawn structure and increase the hydrophobicity and the surface to volume ratio. We hypothesized that such a composite membrane with the frogspawn structure would improve the oil-water separation efficiency and exhibit good durability. The membrane was fully characterized under varied circumstances to investigate its wettability, separation performance and stability. The preparation process, source of inspiration, unique structure, and applications in oil-water separation and the stability of the membrane are illustrated in Fig. 1.

## 2. Materials and methods

### 2.1. Materials

*p*-phenylenediamine (PDA), hydrophobic silica nanoparticles (SNPs) (average particle size 7–40 nm), methyl blue, oil red O, magnesium sulphate, zinc nitrate and soybean oil, HCL were purchased from Shanghai Aladdin Industrial Corporation. 3,3',4,4'-Biphenyltetracarboxylic dianhydride (BPDA) was provided by Changzhou Sunlight Pharmaceutical Co., Ltd. Polydimethylsiloxane (PDMS, average Mw. 115,000) was brought from Dow Corning Silicone Co., Ltd. Dichloromethane, 1,2-dichloroethane, trichloromethane, *n*-hexane, acetone, ether, toluene, chloroform were

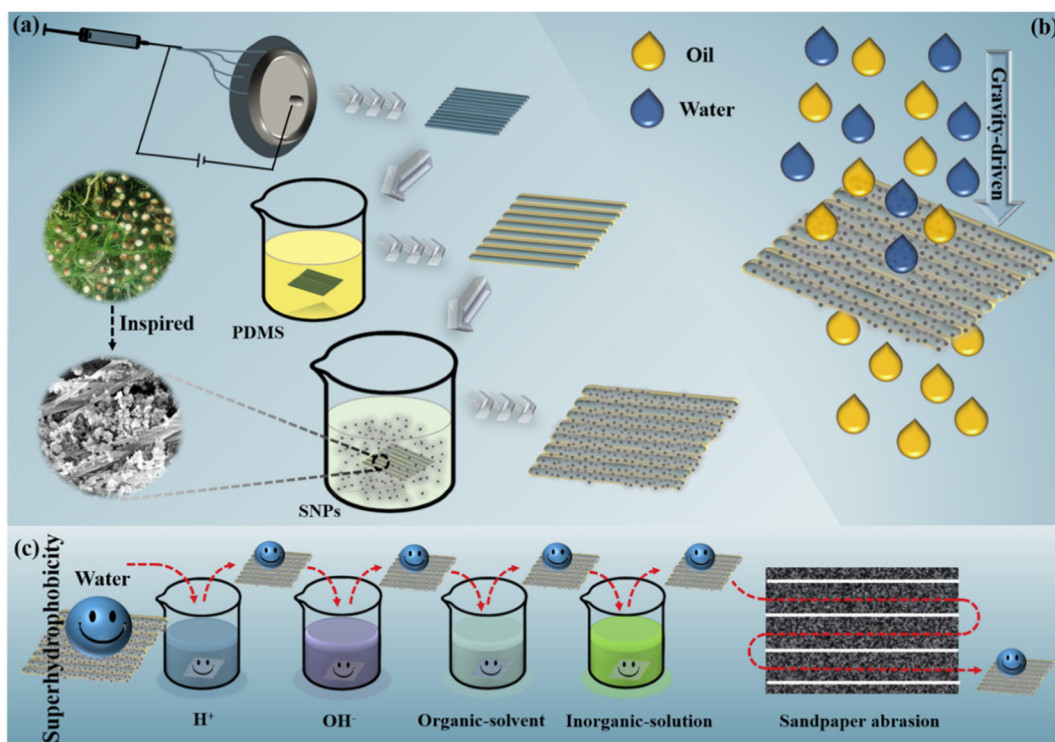


Fig. 1. Illustration of the preparation process (a), separation properties (b) and stability (c).

obtained from Sinopharm Chemical Reagent Co., Ltd. N,N-Dimethylacetamide (DMAC), Tetrahydrofuran (THF), ethyl acetate, bromobenzene, carbon tetrachloride, olive oil, NaOH were purchased from Nanjing Chemical Reagent Co., Ltd. Potassium chloride, calcium chloride, dimethyl sulphoxide were obtained from Shanghai JiuYi Chemical Reagent Co., Ltd. All the purchased reagents were of analytical grade and were used without other treatment, except for *p*-phenylenediamine (PDA) and 3,3',4,4'-Biphenyltetra carboxylic dianhydride (BPDA), which were sublimed *in vacuo* prior to being used for the synthesis of polyamic acid (PAA).

## 2.2. Preparation of the polyimide (PI) membrane

First, *p*-phenylenediamine (PDA) (1.0814 g, 0.01 mol) and 3,3',4,4'-Biphenyltetra carboxylic dianhydride (BPDA) (2.921 g, 0.01 mol) were pre-sublimed to remove the impurities, and then were dissolved in 40 mL N,N-Dimethylacetamide (DMAC), and reacted in the low temperature reactor at  $-5\text{ }^{\circ}\text{C}$  under nitrogen environment for 12 h with constant stirring to form polyamic acid (PAA) [20]. The PAA solution was electrospun using an FM1206 electrospinning device (Beijing Future Material Sci-tech, China) under a voltage of 23 kV (+18 kV,  $-5\text{ kV}$ ), at a rate of  $1\text{ mL h}^{-1}$ . The nanofibres were collected by a rotating wheel-collector with a 15 cm distance from the needle to the collector. The PI membrane was formed by the imidization reaction in a tube furnace under a nitrogen environment. The nanofibres were kept in the furnace for  $150\text{ }^{\circ}\text{C}$ ,  $200\text{ }^{\circ}\text{C}$ ,  $250\text{ }^{\circ}\text{C}$ ,  $300\text{ }^{\circ}\text{C}$  for an hour each and at  $350\text{ }^{\circ}\text{C}$  for 3 h at a heating rate of  $1\text{ }^{\circ}\text{C}/\text{min}$ , and then returned to room temperature gradually. The detailed chemical reaction process is shown in Fig. S1.

## 2.3. Modification of PI membrane

The modification was accomplished using the dip-coating method. The PI membrane was cut into  $2\text{ cm} \times 2\text{ cm}$  pieces prior to being dipped in a polydimethylsiloxane (PDMS) solution (with a varying concentration of 0.1 wt%, 0.5 wt%, 1 wt%, 2 wt%, 4 wt%, respectively) for 2 h continuously. Then, the PDMS was solidified on the surface by drying at  $80\text{ }^{\circ}\text{C}$  for 2 h *in vacuo*, and after this step, the membrane was designated as the PDMS-PI membrane. The PDMS-PI membrane was further modified in a silica nanoparticles (SNPs) suspension (with a varying concentration of 0.1 wt%, 0.5 wt%, 1 wt%, 2 wt%, 4 wt% respectively) for 2 h continuously, and then dried *in vacuo* at  $80\text{ }^{\circ}\text{C}$  for 2 h. The membrane decorated with silica nanoparticles (SNPs) was designated as the PDMS/SNPs-PI membrane. The water contact angle (WCA) of the membrane was measured to obtain the optimum concentration of PDMS and silica nanoparticles (SNPs) in order to fabricate the desired membrane.

## 2.4. Characterization of modified polyimide membrane

The temperature of  $-5\text{ }^{\circ}\text{C}$  was achieved using a low temperature reactor (DFY-5/30, Nanjing Wener China). The pH value was determined using a pH metre (FE20, Mettler Toledo). The functional groups of the membrane were confirmed using a Nicolet 360 FT-IR spectrometer (USA). The surface morphology and structure were investigated using a field emissions scanning electron microscope (FE-SEM) equipped with an energy dispersive spectrometer (EDS) (S-4800, Hitachi, Japan). X-ray powder diffraction (XRD) (Ultima IV, Rigaku, Japan) was applied to examine the structure of the membrane, before and after the modification. Different elements of the membrane surface were examined by X-ray photoelectron spectroscopy (XPS) (AXIS Ultra DLD, UK). Water contact angle (WCA) and oil contact angle (OCA) were measured using a Zhong Chen JC2000D1 contact angle instrument (Shanghai,

China). Thermogravimetric analysis was performed using a thermal gravimetric analyser (TGA Q5000-IR, TA Instruments, USA).

## 2.5. Preparation of oil-water mixture

Petroleum extracts such as dichloromethane, 1,2-dichloroethane, trichloromethane, bromobenzene and carbon tetrachloride were used to test the separation performance of the as-prepared membrane. Oil (10 mL) and water (10 mL) were mixed at a beaker under ultrasonication for 5 min. The oil was dyed with Oil Red O and water was dyed with methyl blue.

## 2.6. Separation testing and evaluation

Separation tests were conducted involving parallel test step ( $n = 3$ ) by pouring a mixture (20 mL) of oil (dichloromethane, 1,2-dichloroethane, trichloromethane, bromobenzene and carbon tetrachloride) and water (50% v/v) into the upper tube, and the oil was collected at a beaker pre-prepared at the bottom. The separation device consists of two measuring cylinder types connected by a flange, with the junction fastened by a clamp. The membrane covered the entire interface between the flange, but only the inner circle area was exposed to the mixture, so that the effective separation area was  $17.6625 \times 10^{-5}\text{ m}^2$  (the inner diameter is 1.5 cm). The flux was calculated based on the time of oil permeation measured 20 times ( $n = 3$ ), and the membrane was reused by drying in room temperature with no other treatment between the cycles. Separation efficiency was calculated as the ratio of the oil weight change. The parameters can be calculated by the following equations:

$$F = \frac{V}{S \cdot T} \quad (1)$$

where  $F$ ,  $V$ ,  $S$ ,  $T$  are the flux, the volume of the permeate phase, the effective contact area of the membrane and the mixture, and the time required for the completion of the separation process, respectively.

$$\eta = \frac{M}{M_0} \times 100\% \quad (2)$$

where  $\eta$ ,  $M$ ,  $M_0$  are the separation efficiency, the weight of the oil after the separation and the initial weight prior to the separation.

## 3. Results and discussion

### 3.1. Functionalization of PI membrane

Field emission scanning electron microscopy was used to observe the surface morphology of the PI (Fig. 2(a)), PDMS-PI (Fig. 2(b)) and PDMS/SNPs-PI (Fig. 2(c)) membranes. It was clear that PDMS shows no influence on the PI fibres, while the frogspawn structure was observed after the silica nanoparticles were decorated on the membrane. It is observed from the SEM images that the pore between the fibres was filled up by the silica nanoparticles, but the multi-pores structure was still preserved. In addition, the changes in the membrane morphologies as function of the concentrations of SNPs are shown in Fig. S2. It was observed that while the SNPs suspension at low concentration was not sufficient for forming the frogspawn structure, the pore of the membrane was blocked when the concentration was too high. The optimum content of PDMS and SNPs for the functionalization of the PI membrane was determined by orthogonal tests, carried out by measuring the water contact angle (WCA) values in air after each modification step. Each sample was measured three times to ensure the accuracy. The WCA values of the PI, PDMS-PI, SNPs/PDMS-PI membranes were  $77.28^{\circ}$ ,  $134.36^{\circ}$  and  $155.75^{\circ}$ , indicating that hydrophobicity increased with the loading

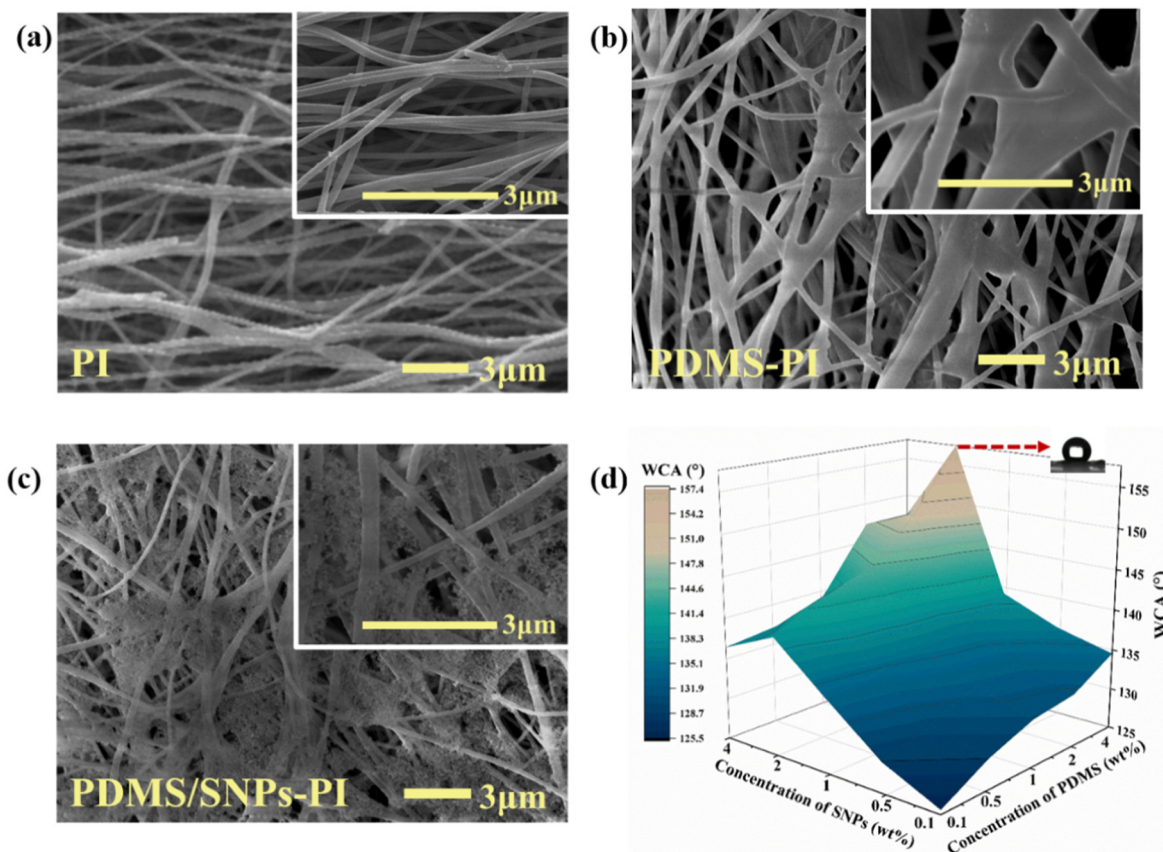


**Fig. 2.** SEM images 5000 $\times$  (insert images was magnified 20,000 $\times$ ) and EDS result. (a) pristine PI membrane, (b) PDMS-PI membrane, (c) PDMS/SNPs-PI membrane, (d) Change in water contact angle with varying concentration of PDMS and silica nanoparticles.

of PDMS and SNPs (Fig. 2(d)). The optimum hydrophobicity was achieved for 4 wt% PDMS and 2 wt% SNPs. Hence, the membranes modified by 4 wt% PDMS and 2 wt% SNPs were used to perform the separation and all the other tests.

The EDS result (Fig. 3(a)) for the PDMS/SNPs-PI membrane also demonstrated the successful modification of silica nanoparticles. The element composition of PDMS/SNPs-PI membrane was confirmed to be C, N, O, Si, because Au was pre-sprayed prior to the SEM characterization to enhance the signal intensity. Additionally, the rough weight content is also provided in Fig. 3(a).

The detailed elemental composition information for the as-prepared membrane was confirmed by XPS. As shown in Fig. 3(b), the PI membrane consisted of C (81.99 at%), N (4.29 at%), O (13.72 at%). Meanwhile Si appeared on the modified membrane, indicates successful incorporation of PDMS and SNPs to the surface of PI membrane. Additionally, it important to mention that the relative percentages of C, N, O, Si of PDMS/SNPs-PI membrane were 48.85, 0.48, 28.21 and 22.46 At%, respectively. The binding energies of 100.5 eV, and 152.5 eV represent the 2p<sub>3/2</sub> and 2s atomic orbitals of Si, respectively [53,54]. Moreover, C1s was detected at 285 eV, which can be further refined as 284.0 eV, 285.5 eV and 286 eV (Fig. 3(c)). The signal at 284.0 eV (54.52 At%) represents the C–H bond and that at 285.5 eV (33.3 At%) corresponds to the sp<sup>2</sup> atomic orbitals and the polarized covalent bond of C and O (C=O) and that at 286 eV (12.18 At%) is the C–N bond because the electronegativity of the N element affected the binding energy position of the C electron orbitals. O1s and N1s signals were found at 532.57 eV and 400.5 eV which showing the presence of PI [55].

Taken together, the XPS results revealed that there were no impurities in the prepared membrane.

Furthermore, XRD was also applied to investigate the structure of the as-prepared membrane. As shown in Fig. 3(d), the peaks at 12° and 24° are ascribed to the characteristic peak of silicon dioxide. However, there were no more characteristic peaks of the regular crystallographic structure because the polymers show amorphous structure [56,57]. In addition, the similar variation tendency suggests that the structure of the membrane was not damaged by the dip-coating process.

Fourier transform infrared spectroscopy was employed to identify the functional groups of the membrane before and after modification. As shown in Fig. 3(e), the adsorption peak at 1771 cm<sup>-1</sup> corresponds to the –CONH stretching vibrations of polyimide, indicating the successful imidization of –COOH with –NH<sub>2</sub> in the PAA fibre. Compared to pristine polyimide membrane, absorption peaks newly appeared at 3466, 2965, 1260, 1085, 795 cm<sup>-1</sup>, corresponding to the stretching vibration of Si–OH (the end group of polydimethylsiloxane) [58], the absorption peak of C–H, the symmetrical stretching vibration (Vs) of Si–CH<sub>3</sub> in the main chain, the asymmetrical stretching vibration (Vas) of Si–O–Si (which is the connection part in the monomers of polydimethylsiloxane) and the absorption peak of Si–CH<sub>3</sub> [59,60], respectively. All these characteristic peaks confirmed the presence of PDMS on the PI fibres. In addition, there was no visible difference between the FTIR spectra of the PDMS-PI membrane and of the PDMS/SNPs-PI membrane, due to the similar chemical bonding of PDMS and SNPs.

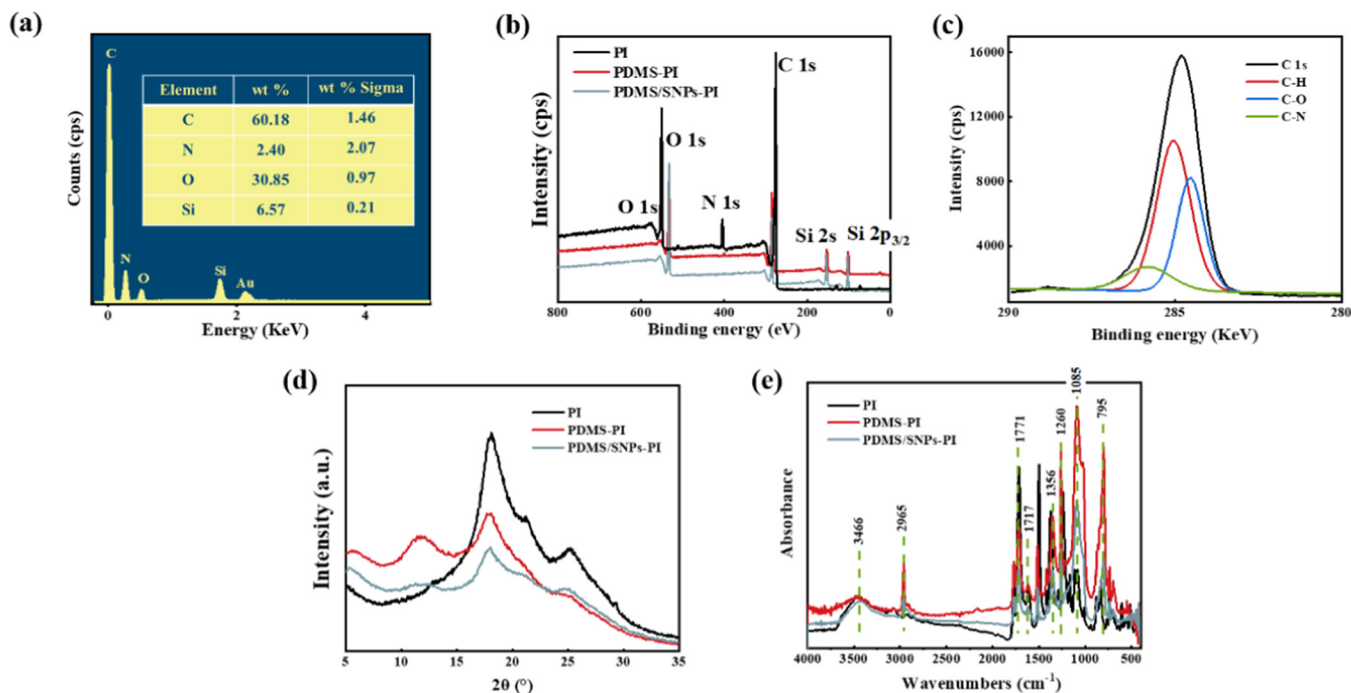


**Fig. 3.** Characterization of PI, PDMS-PI and PDMS/SNPs-PI membrane. (a) EDS result of the PDMS/SNPs-PI membrane (insert table was the element composition of the PDMS/SNPs-PI membrane). (b) XPS spectra, (c) XPS spectra of C 1s. (d) XRD spectra. (e) FTIR spectra.

Based on the above results, the successful incorporation of the PDMS and SNPs onto the PI surface was confirmed. Additionally, the biomimetic structure and superhydrophobic surface were formed after the modification.

### 3.2. Oleophilicity and hydrophobicity of PI membrane

The wettability of the material is a factor that significantly influences the separation ability. Therefore, the surface wettability of the as-prepared membrane was investigated comprehensively. As shown in Fig. 4(a), the water droplet retained a spherical shape on the as-prepared membrane while the dichloromethane was adsorbed immediately, revealing that water-resistance and oil-absorption can be realized simultaneously. In addition, an *n*-hexane droplet (5  $\mu$ L) spread over the surface and then was absorbed immediately (Fig. 4(b)) when contacted with the membrane in air. In contrast, the water droplet can be fully detached from the surface within two seconds without leaving any residual water on the surface of the membrane (Fig. 4(c)), demonstrating the superoleophilicity and the superhydrophobicity of the as-fabricated membrane.

The underwater oleophilicity was another property that must be examined because it can indicate the separation in the droplet level. Hence, the underwater oil contact angle was measured by employing dichloromethane, *n*-hexane, soybean oil and olive oil. As shown in Fig. S3, all the examined types of oil were absorbed by the membrane, especially for dichloromethane and *n*-hexane ( $\theta < 20^\circ$ ). Similarly, the oil (dichloromethane droplet dyed by oil red) was adsorbed by the membrane within four seconds once the membrane was submerged in the water, suggesting the outstanding underwater oleophilicity of the membrane (Fig. 4(d)).

Significantly, the sliding angle that is used measure the difficulty of a water droplet rolling on the membrane, was introduced to examine the superhydrophobicity of the membrane. As displayed in Fig. 4(e), the advancing and receding contact angles on the PDMS/SNPs-PI membranes were measured to be

approximately  $147.08^\circ$  and  $137.83^\circ$ , while the sliding angle of the membrane was measured to be  $9^\circ$ , which is very close to the difference between the advancing and receding contact angles ( $\pm 0.25^\circ$ ). This phenomenon implied that the water can roll off the membrane easily and indicates the superhydrophobicity of the membrane.

### 3.3. Separation performance

To test the efficiencies of the composite membrane in continuous oil-water separation, a device consisting of two glass tube was set up to realize gravity-driven separation. As shown in Fig. 5(a), the mixture was poured into the upper glass, and the oil phase will permeate through the membrane and be collected at a pre-prepared beaker while the water is retained above the as-prepared membrane. The time of oil's permeation and the weight of oil before and after the whole procedure were recorded [61,62]. The separation efficiencies of dichloromethane, 1,2-dichloroethane, trichloromethane, carbon tetrachloride, bromobenzene-water mixture (50%, v/v) were calculated as  $98.81 \pm 0.00278\%$ ,  $99.36 \pm 0.0037\%$ ,  $99.55 \pm 0.0028\%$ ,  $98.07 \pm 0.011\%$ ,  $98.40 \pm 0.0033\%$ , respectively (Fig. 5(b)).

Additionally, the recyclability was investigated with the mixture of water and dichloromethane for 20 cycles. It was found that the mixture was separated thoroughly with the average time of  $44.7 \pm 1.8$  s per cycles with the flux up to  $4443.16 \pm 70.03$  L/ $m^2$  h (Fig. 5(c)). The fluxes of 1,2-dichloroethane, trichloromethane, bromobenzene, carbon tetrachloride-water were 2441, 3500, 1800, 2040 L/ $m^2$  h, respectively, higher than most of the values in the reported work. The varied flux for different oil-water mixtures may ascribed that different pressure on the membrane arise from the different viscosity of the oil. Meanwhile, a high separation efficiency was obtained for all the used oil-water mixtures. In confirmation of the outstanding separation performance of this membrane, flux was chosen as the main factor in the comparison in Fig. S4, all the other work listed were used the same kind of

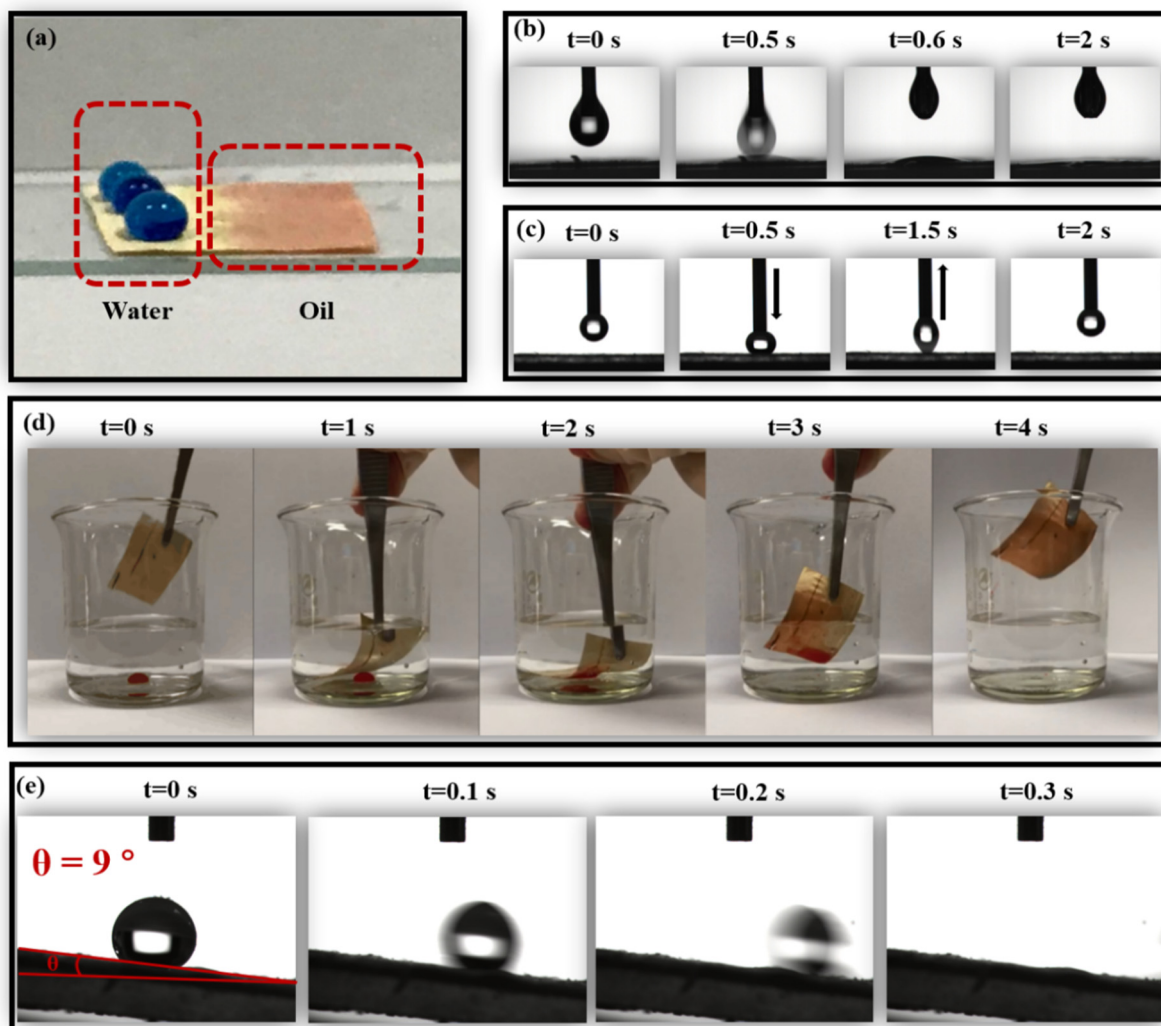


**Fig. 4.** Images of the wettability measurement. (a) Image of water (dye by Methyl blue) and oil (dye by Oil red O) on the membrane surface at the same time. (b) Images of *n*-Hexane dripped on the membrane surface in air. (c) Dynamic images of water pressed on and detached off the membrane surface. (d) Oil being adsorbed by the membrane under water. (e) Images of 5  $\mu\text{L}$  water droplet rolling off the membrane with the sliding angle =  $9^\circ$ .

oil or oil with similar viscosity. For example, the membrane fabricated by PDA/SiO<sub>2</sub> coated cotton fabric, PRCM/PU coated stainless steel mesh, APAN/Ag nanofibre membrane only shows flux values of 4000, 3600, 3250 L/m<sup>2</sup> h, respectively. Even though the flux of this work was not the highest reported, it is still higher than in many previous studies. Interestingly, it is important to mention that the membrane maintained its surface morphology (Fig. S5) even after 20 cycles of separation. The extraordinary recyclability and high efficiency make the as-prepared membrane a promising candidate for practical oil-water separation application.

### 3.4. Separation mechanism

Two wetting states were formed during the different stages of the separation process, providing the connection between the membrane surface structure and separation performance.

The Cassie-Baxter wetting state was first formed as the water contacted the membrane [63]. Due to a thin layer of air bubble occupying the grooves on the surface, the membrane exhibits superhydrophobicity that can be characterized by the following Eqs. (3) and (4):

$$\cos \theta_R = f_{LS} \cos \theta_S - f_{LA} \quad (3)$$

$$f_{LS} + f_{LA} = 1 \quad (4)$$

In Eqs. (3) and (4),  $\theta_R$ ,  $f_{LS}$ ,  $\theta_S$ ,  $f_{LA}$  are the water contact angle in air of the modified membrane, the ratio of the contact area between water and solid to the total area of water on the solid surface, water contact angle in air of the pristine PI membrane and the contact fraction of liquid and air, respectively. The high  $f_{LS}$  correspond to high water contact angle, which means better hydrophobicity. In this work, WCA of the PI, PDMS-PI, PDMS/SNPs-PI membrane were  $77^\circ$ ,  $134^\circ$  and  $155^\circ$ , respectively. The high  $f_{LS}$  correspond to high water contact angle, which means better hydrophobicity. In this work, WCA of the PI, PDMS-PI, PDMS/SNPs-PI membrane were  $77^\circ$ ,  $134^\circ$  and  $155^\circ$ , respectively. The  $f_{LS}$  of PDMS/SNPs-PI membrane were calculated to be 0.323, higher than the  $f_{LS}$  of PDMS-PI membrane 0.249. Hence, we can conclude that the hydrophobicity increased with the modification.

The Cassie-Baxter wetting state was destroyed, and the Wenzel wetting state was formed as the water was added. In this state, the air restored in the grooves starts to be repelled by the water [64], and the wetting behaviour of the membrane can be explained by the following equation:

$$\cos \theta = R \cos \theta_0 \quad (5)$$

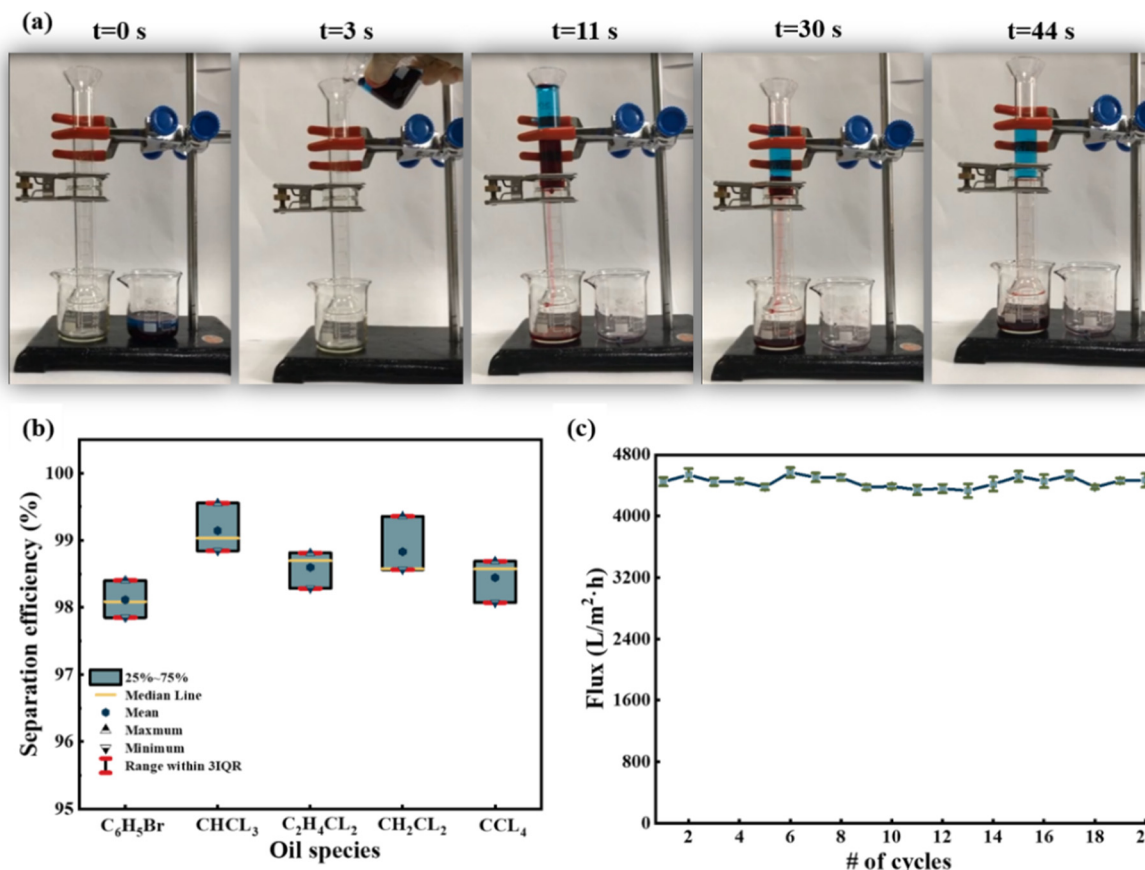


Fig. 5. Separation test and performance evaluation. (a) Images of oil-water separation experiment. (b) Separation efficiency of different kinds of oil ( $n = 3$ ). (c) Flux of 20 cycles (DCM-water, 50% v/v) ( $n = 3$ ).

where  $\theta$  is the water contact angle in air of the relatively rough membrane,  $\theta_0$  is the water contact angle in air of the relatively smooth membrane and  $R$  is the surface roughness factor (the ratio of actual surface area to geometric projection area). The surface roughness factor of PDMS/SNPs-PI membrane is 1.304 for  $\theta = 155^\circ$  and  $\theta_0 = 134^\circ$ , indicating that the actual contact area of liquid and solid interface was large. This phenomenon may be induced by the increase in the surface roughness that was due to the decoration of silica nanoparticles (average size 7–40 nm). The surface roughness was also an important factor affect the wettability and the separation performance. Therefore, the average surface roughness of PDMS/SNPs-PI membrane was measured by white light interferometer to be  $2.025 \mu\text{m}$  (Fig. S6). The high surface roughness increased the contact area of the oil and the membrane which was beneficial for the separation performance.

Even though the contact area increased, the water was still retained at the upper tube. The behaviour of oil was opposite to that of the water, and the oils permeate through the membrane without obstacles. Based on the aforementioned information,  $\Delta p$ , the intrusion pressure from the liquid to the solid surface was introduced as follows: [65]

$$\Delta p = \frac{2\gamma}{R} = -\frac{L\gamma \cos \theta}{A} \quad (6)$$

where  $\Delta p$ ,  $\gamma$ ,  $R$ ,  $L$ ,  $\theta$ ,  $A$  are the intrusion pressure, the surface tension, the radius of the meniscus, the perimeter of the pore on the membrane, the contact angle in air cross-section area and the cross-section area of the pore on the membrane, respectively. The intrusion pressure of water  $> 0$ , indicating that the membrane can bear the pressure induced by water. Conversely, the oil contact angle in

air was  $5.7^\circ$ , resulting the  $\Delta p < 0$ , so that the membrane cannot bear the pressure induced by oil, leading to the permeation of oil. The separation can be achieved when the oil permeates through the membrane while the water was intercepted.

### 3.5. Stability and durability of composite PI membrane

The stability of the separation material was another parameter that must be considered because the environment can be complex in the real oil-water separation applications. Thus, a series of experiments were designed to test the stability characteristics of the membrane such as thermal stability and chemical stability (including varied pH values and different chemicals exposure). The change in the membrane weight as a function of temperature was studied using TGA curves. As shown in Fig. 6(a), the composite membrane had a weight loss of only 3% below  $100^\circ\text{C}$ , which may be attributed to the release of the water contained in the sample. It is important to mention that only approximately 10% weight loss was observed approximately  $500^\circ\text{C}$  and the membrane retained 40% of its initial weight at  $800^\circ\text{C}$ , suggesting the excellent thermal stability of the as-fabricated membrane.

Moreover, WCA was measured at different pH values from 1 to 14 to study the stability of the membrane. The acid and alkaline environment were obtained using either an HCl or a NaOH aqueous solutions. As shown in Fig. 6(b), the WCA values fluctuate around the  $150^\circ$ , indicated the pH-stability of the hydrophobicity. Furthermore, the chemical stability was studied by immersing the membrane into ten kinds of solutions including *n*-hexane, acetone, ether, toluene, chloroform, dimethyl sulphoxide, KCl (1 mol/L), CaCl<sub>2</sub> (1 mol/L), MgSO<sub>4</sub> (1 mol/L), and ZnNO<sub>3</sub> (1 mol/L) for 24 h

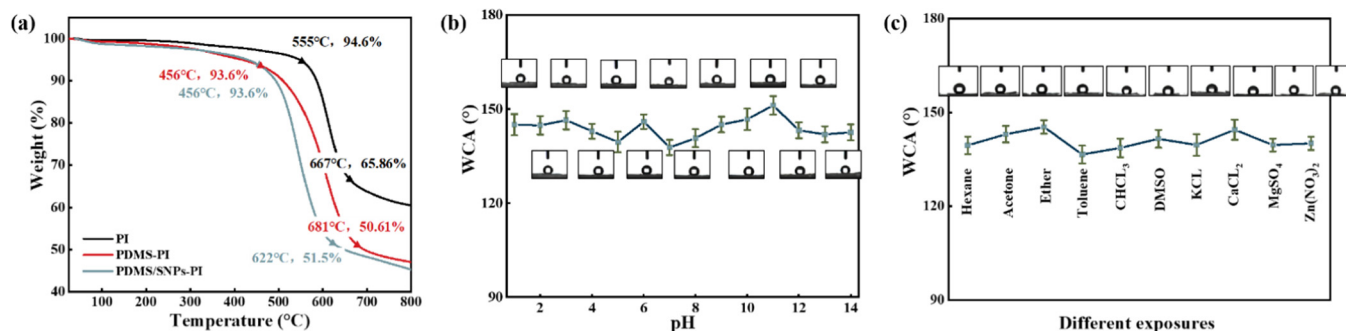


**Fig. 6.** Stability of the membrane. (a) TGA curves of PI membrane, PDMS/PI membrane and PDMS-SNPs/PI membrane. WCA measured ( $n = 3$ ) at different temperature (b), different pH values (c), after immersing into different solutions for 24 h (d).

(Fig. 6(c)). Neither the organic solvent nor the inorganic salt solution changed the superhydrophobicity of the as-prepared membrane, fully demonstrating the good chemical resistance of the as-prepared membrane.

In addition to chemical stability, the mechanical property was another factor that should be considered. The anti-abrasion test was performed by a sliding membrane on the surface of sandpapers (500, 1000, 2000 mesh) as a square (15 cm border side) with 100 g weight applied for 10 cycles. The images of the experiment and surface morphologies before and after the abrasion test are shown in Fig. S7. The abrasion of 2000 mesh sandpaper nearly shows no influences on the surface morphology. However, the membrane abraded by 500 mesh lost most of its frogspawn structure. Even though the nanofibres were subjected to different levels of damages through destruction, the membrane still shows excellent anti-abrasion property, further confirming that the membrane was sufficiently stable for applications in various conditions.

#### 4. Conclusion

In this work, a strategy was proposed to fabricate hierarchical frogspawn-structure membrane by the combination of electrospinning technology and dip-coating method in order to solve oily wastewater pollution purification problem. The easy preparation process and energy-saving separation membrane paves the way for massive production of functional membranes. The oil-water mixture can be separated thoroughly without an additional energy input and the recyclability together with the separation performance of the membrane was well behaved. Furthermore, the membrane is highly stable under complex environments, such as acid, alkaline, and organic/inorganic solvent can be tolerant. All these properties showed that superior to many membranes reported in previous publications [66,67]. Our study suggests that the obtained membrane may have versatile applications in water purification, oil collection, and liquid separation, which remains a key challenge in field of oily wastewater pollution.

#### Acknowledgement

Funding for this work was provided by National Key R&D Program of China (2017YFF0207804), National Natural Science Foundation of China (No. 21774060), Jiangsu key lab of biomass-based energy and Materials (JSBEM2016011), State Key Laboratory for Mechanical Behavior of Materials (20171914), Priority Academic Program Development of Jiangsu Higher Education Institutions (PAPD), Top-notch Academic Programs Project of Jiangsu Higher Education Institutions (TAPP) and Natural Science Key Project of the Jiangsu Higher Education Institutions (16KJA220006). The

authors acknowledge Advanced Analysis & Testing Center, Nanjing Forestry University for SEM, XPS, XRD characterization.

#### Appendix A. Supplementary material

Supplementary data to this article can be found online at <https://doi.org/10.1016/j.jcis.2019.03.099>.

#### References

- [1] E. Stokstad, Gulf oil disaster. Looking beyond the spill, Obama highlights long-term restoration, *Science* 328 (2010) 1618–1619.
- [2] D. Fragouli, A. Athanassiou, Oil spill recovery: graphene heaters absorb faster, *Nat. Nanotechnol.* (2017) 406–407.
- [3] J.E. Kostka, O. Prakash, W.A. Overholt, S.J. Green, G. Freyer, A. Canion, J. Delgado, N. Norton, T.C. Hazen, M. Huettel, Hydrocarbon-degrading bacteria and the bacterial community response in gulf of mexico beach sands impacted by the deepwater horizon oil spill, *Appl. Environ. Microbiol.* 77 (2011) 7962–7974.
- [4] D. Lockwood, Environment Sanchi oil spill continues; impacts still unclear, *Chem. Eng. News* 96 (2018). 16 16.
- [5] L.P. Yin, M. Zhang, Y.L. Zhang, F.L. Qiao, The long-term prediction of the oil-contaminated water from the Sanchi collision in the East China Sea, *Acta Oceanol. Sinica* 37 (2018) 69–72.
- [6] T.A. Saleh, A.A. Al-Absi, Kinetics, isotherms and thermodynamic evaluation of amine functionalized magnetic carbon for methyl red removal from aqueous solutions, *J. Mol. Liq.* 248 (2017) 577–585.
- [7] T.A. Saleh, M. Tuzen, A. Sari, Polyamide magnetic polygorskite for the simultaneous removal of Hg(II) and methyl mercury: with factorial design analysis, *J. Environ. Manage.* 211 (2018) 323–333.
- [8] M. Tuzen, A. Sari, T.A. Saleh, Response surface optimization, kinetic and thermodynamic studies for effective removal of rhodamine B by magnetic AC/CeO<sub>2</sub> nanocomposite, *J. Environ. Manage.* 206 (2018) 170–177.
- [9] Y. Liu, B. Zhan, K.T. Zhang, C. Kaya, T. Stegmaier, Z.W. Han, L.Q. Ren, On-demand oil/water separation of 3D Fe foam by controllable wettability, *Chem. Eng. J.* 331 (2018) 278–289.
- [10] J. Xiao, W. Lv, Y. Song, Q. Zheng, Graphene/nanofiber aerogels: performance regulation towards multiple applications in dye adsorption and oil/water separation, *Chem. Eng. J.* 338 (2018).
- [11] Y.F. Si, L.W. Chen, F.C. Yang, F. Guo, Z.G. Guo, Stable Janus superhydrophilic/hydrophobic nickel foam for directional water transport, *J. Colloid Interface Sci.* 509 (2018) 346–352.
- [12] J.P. Zhang, S. Seeger, Polyester materials with superwetting silicone nanofilaments for oil/water separation and selective oil absorption, *Adv. Funct. Mater.* 21 (2011) 4699–4704.
- [13] M. Yeber, E. Paul, C. Soto, Chemical and biological treatments to clean oily wastewater: optimization of the photocatalytic process using experimental design, *Desalin. Water Treat.* 47 (2012) 295–299.
- [14] C.F. Komives, E. Lilley, A.J. Russell, Biodegradation of pesticides in nonionic water-in-oil microemulsions of tween 85: relationship between micelle structure and activity, *Biotechnol. Bioeng.* 43 (1994) 946–959.
- [15] Q. Huang, H. Xu, F. Mao, C. Yong, J. Yan, Effect of the particle surface on oil recovery from petroleum sludge, *Energy Fuels* 28 (2014) 4480–4485.
- [16] X. Xu, X. Zhu, Treatment of refractory oily wastewater by electro-coagulation process, *Chemosphere* 56 (2004) 889–894.
- [17] W.J. Ma, M.J. Zhang, Z.C. Liu, M.M. Kang, C.B. Huang, G.D. Fu, Fabrication of highly durable and robust superhydrophobic-superoleophilic nanofibrous membranes based on a fluorine-free system for efficient oil/water separation, *J. Membr. Sci.* 570 (2019) 303–313.
- [18] Z. Chu, S. Seeger, Superamphiphobic surfaces, *Chem. Soc. Rev.* 43 (2014) 2784–2798.

- [19] A. Rezaee Shirin-Abadi, M. Gorji, S. Rezaee, P.G. Jessop, M.F. Cunningham, CO<sub>2</sub>-Switchable-hydrophilicity membrane (CO<sub>2</sub>-SHM) triggered by electric potential: faster switching time along with efficient oil/water separation, *Chem Commun (Camb)* (2018).
- [20] W. Ma, J. Zhao, O. Oderinde, J. Han, Z. Liu, B. Gao, R. Xiong, Q. Zhang, S. Jiang, C. Huang, Durable superhydrophobic and superoleophilic electrospun nanofibrous membrane for oil-water emulsion separation, *J Colloid Interface Sci* 532 (2018) 12–23.
- [21] Y. Liu, K. Zhang, Y. Son, W. Zhang, L.M. Spindler, Z. Han, L. Ren, A smart switchable bioinspired copper foam responding to different pH droplets for reversible oil-water separation, *J. Mater. Chem. A* 5 (2017) 2603–2612.
- [22] Y. Li, X. Zheng, Z. Yan, X. Zhang, D. Tian, J. Ma, L. Jiang, Closed pore structured NiCo<sub>2</sub>O<sub>4</sub> coated nickel foam for stable and effective oil/water separation, *ACS Appl. Mater. Interfaces* (2017).
- [23] Z. Lei, G. Zhang, Y. Deng, C. Wang, Surface modification of melamine sponges for pH-responsive oil adsorption and desorption, *Appl. Surf. Sci.* 416 (2017) 798–804.
- [24] Z. Lei, G. Zhang, Y. Deng, C. Wang, Thermoresponsive melamine sponges with switchable wettability by interface-initiated atom transfer radical polymerization for oil/water separation, *ACS Appl. Mater. Interfaces* 9 (2017) 8967–8974.
- [25] J. Wang, W. Zhang, Y. Qian, B. Deng, W. Tian, pH, temperature, and magnetic triple-responsive polymer porous microspheres for tunable adsorption, *Macromol. Mater. Eng.* 301 (2016) 1132–1141.
- [26] W. Ma, Z. Guo, J. Zhao, Q. Yu, F. Wang, J. Han, H. Pan, J. Yao, Q. Zhang, S.K. Samal, S.C. De Smedt, C. Huang, Polyimide/cellulose acetate core/shell electrospun fibrous membranes for oil-water separation, *Separat. Purif. Technol.* 177 (2017) 71–85.
- [27] J. Li, C.C. Xu, C.Q. Guo, H.F. Tian, F. Zha, L. Guo, Underoil superhydrophilic desert sand layer for efficient gravity-directed water-in-oil emulsions separation with high flux, *J. Mater. Chem. A* 6 (2018) 223–230.
- [28] F. Li, Z.X. Yu, H. Shi, Q.B. Yang, Q. Chen, Y. Pan, G.Y. Zeng, L. Yan, A Mussel-inspired method to fabricate reduced graphene oxide/g-C<sub>3</sub>N<sub>4</sub> composites membranes for catalytic decomposition and oil-in-water emulsion separation, *Chem. Eng. J.* 322 (2017) 33–45.
- [29] R.P. Lively, D.S. Sholl, From water to organics in membrane separations, *Nat. Mater.* 16 (2017) 276–279.
- [30] W. Ma, Q. Zhang, D. Hua, R. Xiong, J. Zhao, W. Ra, S. Huang, X. Zhan, F. Chen, C. Huang, Electrospun fibers for oil-water separation, *RSC Adv.* 6 (2016) 12868–12884.
- [31] X. Wang, J. Yu, G. Sun, B. Ding, Electrospun nanofibrous materials: a versatile medium for effective oil/water separation, *Mater. Today* 19 (2016) 403–414.
- [32] A. Reina, X. Jia, J. Ho, D. Nezich, H. Son, V. Bulovic, M.S. Dresselhaus, J. Kong, Large area, few-layer graphene films on arbitrary substrates by chemical vapor deposition, *Nano Lett.* 9 (2009) 30–35.
- [33] Y. Wang, Y. Shi, L. Pan, M. Yang, L. Peng, S. Zong, Y. Shi, G. Yu, Multifunctional superhydrophobic surfaces templated from innately microstructured hydrogel matrix, *Nano Lett.* 14 (2014) 4803–4809.
- [34] J. Ge, D. Zong, Q. Jin, J. Yu, B. Ding, Biomimetic and superwetable nanofibrous skins for highly efficient separation of oil-in-water emulsions, *Adv. Funct. Mater.* 1705051 (2018).
- [35] W.J. Ma, M.J. Zhang, Z.C. Liu, C.B. Huang, G.D. Fu, Nature-inspired creation of a robust free-standing electrospun nanofibrous membrane for efficient oil-water separation, *Environ.-Sci. Nano* 5 (2018) 2909–2920.
- [36] M.S. Islam, J.R. McCutcheon, M.S. Rahaman, A high flux polyvinyl acetate-coated electrospun nylon 6/SiO<sub>2</sub> 2 composite microfiltration membrane for the separation of oil-in-water emulsion with improved antifouling performance, *J. Membr. Sci.* 537 (2017) 297–309.
- [37] A. Raza, B. Ding, G. Zainab, M. Elnewehy, S. Aldeyab, J. Yu, In situ cross-linked superwetting nanofibrous membranes for ultrafast oil-water separation, *J. Mater. Chem. A* 2 (2014) 10137–10145.
- [38] X. Dai, Y. Cao, X. Shi, X. Wang, The PLA/ZIF-8 nanocomposite membranes: the diameter and surface roughness adjustment by ZIF-8 nanoparticles, high wettability, improved mechanical property, and efficient oil/water separation, *Adv. Mater. Interfaces* 3 (2016) 1600725.
- [39] W. Panatdasirisuk, Z. Liao, T. Vongsetskul, S. Yang, Separation of Oil-in-water emulsions using hydrophilic electrospun membranes with anisotropic pores, *Langmuir: the ACS J Surf. Colloids* 33 (2017) 5872–5878.
- [40] J. Wu, A.K. An, J. Guo, E.-J. Lee, M.U. Farid, S. Jeong, CNTs reinforced superhydrophobic-oleophilic electrospun polystyrene oil sorbent for enhanced sorption capacity and reusability, *Chem. Eng. J.* 314 (2017) 526–536.
- [41] L. Hu, S.J. Gao, Y.Z. Zhu, F. Zhang, L. Jiang, J. Jin, An ultrathin bilayer membrane with asymmetric wettability for pressure responsive oil/water emulsion separation, *J. Mater. Chem. A* 3 (2015) 23477–23482.
- [42] Hu Liang, Shoujian Gao, Xianguang Ding, Dong Wang, Jiang Jiang, Jian Jin, L. Jiang, Photothermal-responsive single-walled carbon nanotube-based ultrathin membranes for on/off switchable separation of oil-in-water nanoemulsions, *ACS Nano* (2015) 4835–4842.
- [43] D. Tian, X. Zhang, Y. Tian, Y. Wu, X. Wang, J. Zhai, L. Jiang, Photo-induced water-oil separation based on switchable superhydrophobicity-superhydrophilicity and underwater superoleophobicity of the aligned ZnO nanorod array-coated mesh films, *J. Mater. Chem.* 22 (2012) 19652.
- [44] C. Cao, M. Ge, J. Huang, S. Li, S. Deng, S. Zhang, Z. Chen, K. Zhang, S.S. Al-Deyab, Y. Lai, Robust fluorine-free superhydrophobic PDMS-ormosil@fabrics for highly effective self-cleaning and efficient oil-water separation, *J. Mater. Chem. A* 4 (2016) 12179–12187.
- [45] Z. Xu, Y. Zhao, H. Wang, H. Zhou, C. Qin, X. Wang, T. Lin, Fluorine-free superhydrophobic coatings with pH-induced wettability transition for controllable oil-water separation, *ACS Appl. Mater. Interfaces* 8 (2016) 5661–5667.
- [46] Q.Y. Cheng, C.S. Guan, M. Wang, Y.D. Li, J.B. Zeng, Cellulose nanocrystal coated cotton fabric with superhydrophobicity for efficient oil/water separation, *Carbohydr. Polym.* 199 (2018) 390–396.
- [47] L.H. Xu, Y. He, X. Feng, F.Y. Dai, N. Yang, Y.P. Zhao, L. Chen, A comprehensive description of the threshold flux during oil/water emulsion filtration to identify sustainable flux regimes for tannic acid (TA) dip-coated poly(vinylidene fluoride) (PVDF) membranes, *J. Membr. Sci.* 563 (2018) 43–53.
- [48] Q.Y. Cheng, X.P. An, Y.D. Li, C.L. Huang, J.B. Zeng, Sustainable and biodegradable superhydrophobic coating from epoxidized soybean oil and ZnO nanoparticles on cellulose substrates for efficient oil/water separation, *ACS Sustain. Chem. Eng.* 5 (2017) 11440–11450.
- [49] S. Gaidukovs, A. Medvids, P. Onufrijevs, L. Grase, UV-light-induced curing of branched epoxy novolac resin for coatings, *Express Polym. Lett.* 12 (2018) 918–929.
- [50] B. Ding, H.Y. Kim, S.C. Lee, C.L. Shao, D.R. Lee, S.J. Park, G.B. Kwag, K.J. Choi, Preparation and characterization of a nanoscale poly(vinyl alcohol) fiber aggregate produced by an electrospinning method, *J. Polym. Sci. Part B-Polym. Phys.* 40 (2002) 1261–1268.
- [51] Q. Li, A.K. Mishra, N.H. Kim, T. Kuila, K.T. Lau, J.H. Lee, Effects of processing conditions of poly(methylmethacrylate) encapsulated liquid curing agent on the properties of self-healing composites, *Compos. Part B-Eng.* 49 (2013) 6–15.
- [52] H. Haoqing, X.U. Wenhui, D. Yichun, The recent progress on high-performance polymer nanofibers by electrospinning, *J. Jiangxi Normal University(Natural Science Edition)* (2018).
- [53] Y. Liu, H.M. Gu, Y. Jia, J. Liu, H. Zhang, R.M. Wang, B.L. Zhang, H.P. Zhang, Q.Y. Zhang, Design and preparation of biomimetic polydimethylsiloxane (PDMS) films with superhydrophobic, self-healing and drag reduction properties via replication of shark skin and SI-ATRP, *Chem. Eng. J.* 356 (2019) 318–328.
- [54] S. Watcharotone, D.A. Dikin, S. Stankovich, R. Piner, I. Jung, G.H.B. Dommett, G. Evmenenko, S.E. Wu, S.F. Chen, C.P. Liu, S.T. Nguyen, R.S. Ruoff, Graphene-silica composite thin films as transparent conductors, *Nano Lett.* 7 (2007) 1888–1892.
- [55] H.W. Ha, A. Choudhury, T. Kamal, D.H. Kim, S.Y. Park, Effect of chemical modification of graphene on mechanical, electrical, and thermal properties of polyimide/graphene nanocomposites, *ACS Appl. Mater. Interfaces* 4 (2012) 4623–4630.
- [56] Y. Amada, Y. Shinmi, S. Koso, T. Kubota, Y. Nakagawa, K. Tomishige, Reaction mechanism of the glycerol hydrogenolysis to 1,3-propanediol over Ir-ReO<sub>x</sub>/SiO<sub>2</sub> catalyst, *Appl. Catal. B* 105 (2011) 117–127.
- [57] Y. Qing, Z. Zenan, K. Deyu, C. Rongshen, Influence of nano-SiO<sub>2</sub> addition on properties of hardened cement paste as compared with silica fume, *Constr. Build. Mater.* 21 (2007) 539–545.
- [58] T.A. Saleh, Isotherm, kinetic, and thermodynamic studies on Hg(II) adsorption from aqueous solution by silica-multiwall carbon nanotubes, *Environ. Sci. Pollut. Res.* 22 (2015) 16721–16731.
- [59] T.A. Saleh, Nanocomposite of carbon nanotubes/silica nanoparticles and their use for adsorption of Pb(II): from surface properties to sorption mechanism, *Desalin. Water Treat.* 57 (2015) 10730–10744.
- [60] T.A. Saleh, Mercury sorption by silica/carbon nanotubes and silica/activated carbon: a comparison study, *J. Water Supply Res. Technol. AQUA* 64 (2015) 892–903.
- [61] N. Baig, T.A. Saleh, Initiator-free natural light-driven vapor phase synthesis of a porous network of 3D polystyrene branched carbon nanofiber grafted polyurethane for hexane /water separation, *ChemistrySelect* 3 (2018) 8312–8318.
- [62] N. Baig, T.A. Saleh, Natural-light-initiated 3D macro zigzag architecture of graphene-reinforced polystyrene for gravity-driven oil and water separation, *Global Challenges* 2 (2018) 1800040.
- [63] F. Zhang, W.B. Zhang, Z. Shi, D. Wang, J. Jin, L. Jiang, Nanowire-haired inorganic membranes with superhydrophilicity and underwater ultralow adhesive superoleophobicity for high-efficiency oil/water separation, *Adv. Mater.* 25 (2013) 4192–4198.
- [64] P. Gupta, B. Kandasubramanian, Directional fluid gating by janus membranes with heterogeneous wetting properties for selective oil-water separation, *ACS Appl. Mater. Interfaces* 9 (2017) 19102–19113.
- [65] X.F. Gao, L.P. Xu, Z.X. Xue, L. Feng, J.T. Peng, Y.Q. Wen, S.T. Wang, X.J. Zhang, Dual-scaled porous nitrocellulose membranes with underwater superoleophobicity for highly efficient oil/water separation, *Adv. Mater.* 26 (2014) 1771–1775.
- [66] C. Zheng, G. Liu, H. Hu, UV-curable antimud coatings, *ACS Appl. Mater. Interfaces* (2017).
- [67] J. Zhang, Q. Xue, X. Pan, Y. Jin, W. Lu, D. Ding, Q. Guo, Graphene oxide/polyacrylonitrile fiber hierarchical-structured membrane for ultra-fast microfiltration of oil-water emulsion, *Chem. Eng. J.* 307 (2017) 643–649.